A Collaborative Mixed Reality Platform for the Planning of Vascular Surgery

Jing-Yuan Wang
Department of Mathematics
University of Macau
Macau, China

Yujie Gong
Department of Mathematics
University of Macau
Macau, China

Jie Zhou
Department of Mathematics
University of Macau
Macau, China

Fenfen Qi
Department of Mathematics
University of Macau
Macau, China

Yingzhi Liu
Department of Mathematics
University of Macau
Macau, China

Zaiheng Cheng
Shenzhen Institute of Advanced Technology
Chinese Academy of Sciences
Shenzhen, Guangdong, China

Rongliang Chen
Shenzhen Institute of Advanced Technology
Chinese Academy of Sciences
Shenzhen, Guangdong, China

Xinhong Wang
Department of Radiology
The Second Affiliated Hospital
Zhejiang University School of Medicine
Hangzhou, Zhejiang, China

Li Luo
Department of Mathematics
University of Macau
Macau, China

Xiao-Chuan Cai
Department of Mathematics
University of Macau
Macau, China

***Abstract*—In this paper, we develop a mixed reality (MR) platform for the collaborative visualization and manipulation of 3D images of the human body and the control of numerical simulations for the purpose of surgical planning for certain vascular diseases. The MR platform allows multiple users to view and make changes of virtual objects in a server/client fashion in real time. The input of the system is the images of a human body obtained from MRI scans and segmentations of some of the organs are obtained as a pre-processing step. The interaction of the physical hands and the virtual objects are carried out through several pairs of holographic devices equipped with hand gesture recognition. For each planned surgical configuration, the corresponding hemodynamics is analyzed via a connected supercomputer whose output is transferred back to the controlling holographic devices. As an example, we consider the surgical planning of the type B aortic dissection. This is a rather complex procedure and the proposed mixed reality platform is used to visually study several possible placement of a stent. In addition to visualization, the platform also provides near real time computation of the blood flows corresponding to each of the planned surgical scenarios, and the computation is controlled by hand gestures from the holographic devices.**

***Index Terms*—Collaborative mixed reality, interactive control by holographic devices, surgical planning, computational hemodynamics, abdominal aorta, parallel computing**

I. Introduction

In recent years, the development of virtual, augmented, and mixed reality technologies (VR/AR/MR, or collectively called XR), has witnessed remarkable progress, and the impact of the technologies continues to grow, thanks to their capabilities for creating captivating three-dimensional (3D) digital environments. These interactive and immersive technologies have seen increasing adoption in various industries such as video gaming, commerce, education, and healthcare.

Traditional imaging technologies in medical sciences such as CT and MRI produce sequences of 2D slices that can be combined together to reconstruct a 3D representation of the region of interest. By utilizing holographic devices, users are able to directly view and interact with these 3D virtual objects from any angle and location. This significantly enhances the viewing experience and improves the accuracy of diagnosis and surgical planning. Numerous studies have demonstrated the potential of XR in various biomedical applications. For instance, Hanna et al. [1] showcased the possibilities of AR in pathology, emphasizing its applications in virtual annotation and 3D specimen viewing. Serrano et al. [2] conducted a study comparing AR and VR setups for anatomy training, uncovering their distinctions. A comprehensive overview of existing biomedical applications was provided in [3]. In [4], the authors explored the integration of these technologies in surgical training, patient care, and surgical practices. More recently, references [5] and [6] highlighted the benefits of telementoring through the metaverse in surgical practice. Wang et al. [7] validated the technical feasibility and effectiveness of a MR neurosurgical training system for preoperative planning. Researchers have also investigated the application of these technologies involving specific organs such as the brain [8], heart [9], and kidneys [10].

While virtual environments are primarily designed for single-user applications, there is a growing emphasis on collaborative techniques [7], [11], [12] that enable multiple users to actively participate in and manipulate virtual objects together within a shared or isomorphic virtual environment,

The research is supported in part by FDCT 0141/2020/A3, 0079/2021/AFJ, 0090/2022/A2.

979-8-3315-1599-7/24/$31.00 ©2024 IEEE
DOI 10.1109/MetaCom62920.2024.00017

regardless of whether they are co-located or remotely connected. For instance, a collaborative VR environment specifically designed for liver surgery was introduced in [13]–[15]. However, this VR-based system prevents users from maintaining awareness of their real-world surroundings. To enhance the integration of the virtual object with the user's physical environment, we propose a collaborative MR platform in this work.

With the rapid development of computing technology, numerical simulation has become a powerful tool to study surgical outcomes. It is increasingly employed in various biomechanical applications due to its non-invasiveness and flexibility. However, such computations are often large and complex and can't be conducted directly in the holographic devices that have limited memory and computing capabilities. Efforts have been made to design a platform such that the control of the computation is handled by the holographic devices, but the actual computation is performed on a cluster of computers wirelessly connected to the devices. Mathematical modeling and VR simulation of some surgical procedures were introduced in [16], [17]. In [9], Gong et al. developed a hyperelasticity model for the digital human heart and an interactive platform for visualization, where a high-performance computer cluster was used as the workhorse for heavy computations.

Advancements in medical imaging technology and scientific computing have facilitated the simulation of blood flow in complex arterial networks, enabling the estimation of hemodynamic indicators, and understanding of multi-organ interactions [18]–[20]. In the present work, we focus on hemodynamics simulation of some cardiovascular diseases such as aortic aneurysm and dissection [21]. More specifically, we consider the surgical planning of a patient with a type B aortic dissection and demonstrate how the numerical simulation is incorporated into the proposed collaborative MR platform. The blood flow is modeled by the incompressible Navier-Stokes equations, which are discretized using a finite element method on an unstructured mesh. To address the computational challenges, we develop a scalable and robust algorithm based on the Newton-Krylov-Schwarz (NKS) framework to achieve near real-time simulations when executed on a parallel computer [22], [23]. The computed velocity and pressure values provide valuable insights into the optimal placement of stents within the aorta during the surgical planning procedure.

The rest of the article is organized as follows. Section II provides an introduction to the proposed interactive platform, including the implementation details of holographic interaction and collaboration. It also covers the vascular model and the parallel method used for numerical simulation. In Section III, we present the workflow of surgical planning for stent deployment in an aorta and the corresponding prediction results. Finally, Section IV offers some concluding remarks and discusses potential future work.

II. A COLLABORATIVE PLATFORM FOR SURGICAL PLANNING

Figure 1 presents the basic components of the proposed collaborative mixed reality platform, which includes multiple pairs of holographic devices, a platform manager (PM), a human and his digital twin overlapping each other on the operating table, and a parallel cluster serving as the computational engine. The platform allows participants to simultaneously view the same digital human body, manipulate various model components, perform virtual surgeries by pre-defined hand-gestures recognizable by the holographic devices, and predict potential surgical outcomes, both users in the same laboratory (Figure 1(a)) and from a remote location (Figure 1(b)). One of the notable features of this platform is the ability to maintain the user to user eye contact as well as the users eye contact with the physical environment, this is important for the effective communication among users when planning a complex surgery. It is worth noting that Figure 1(a) is captured by the fourth user in the blue dashed box. The platform manager (PM), as depicted in Figure 1(d), acts as an intermediary to input data from the holographic devices and to coordinate the numerical simulation on the computational engine 1(f). For instance, if the users deploy a stent in an artery as shown in Figure 1(c), the PM issues the related commands to the computational engine for simulation. Subsequently, results from the computation are relayed back to the PM, and then rendered by the users' devices. In this platform, the PM consists of a small cluster of GPUs, while the computational engine is constructed using a large number of CPUs. Each user's holographic device is wirelessly connected with a GPU station and the hand-gestures based operations of one user can be communicated to other users via a transmission control protocol (TCP) connection. Since a large amount of data needs to be sent back and forth between the PM and the computational engine, a fiber optic connection is necessary.

The detailed process of MR-based surgical planning systems illustrated in Figure 2. A group of surgeons, each wearing a pair of holographic glasses, can view the real and virtual objects through their glasses and can also manipulate the virtual objects and control certain computational tasks through hand-gestures. Hand-gestures captured by the cameras are then transmitted to the device manager and synchronized by the PM for further actions. On the top right part of Figure 2, we show other important elements of the system. To prepare for the holographic devices, patient's image data is obtained beforehand, and it undergoes segmentation and reconstruction so that only the region and organ of interests are loaded to the glasses, not the raw image data. To prepare for the numerical computation, a mesh is created for the reconstructed geometry to enable finite element analysis, and both the mesh and the mathematical model are loaded into the PM. Different aspects of the computational results are provided to users to help the surgical planning. Real-time surgical planning requires a powerful computational engine capable of parallel processing.

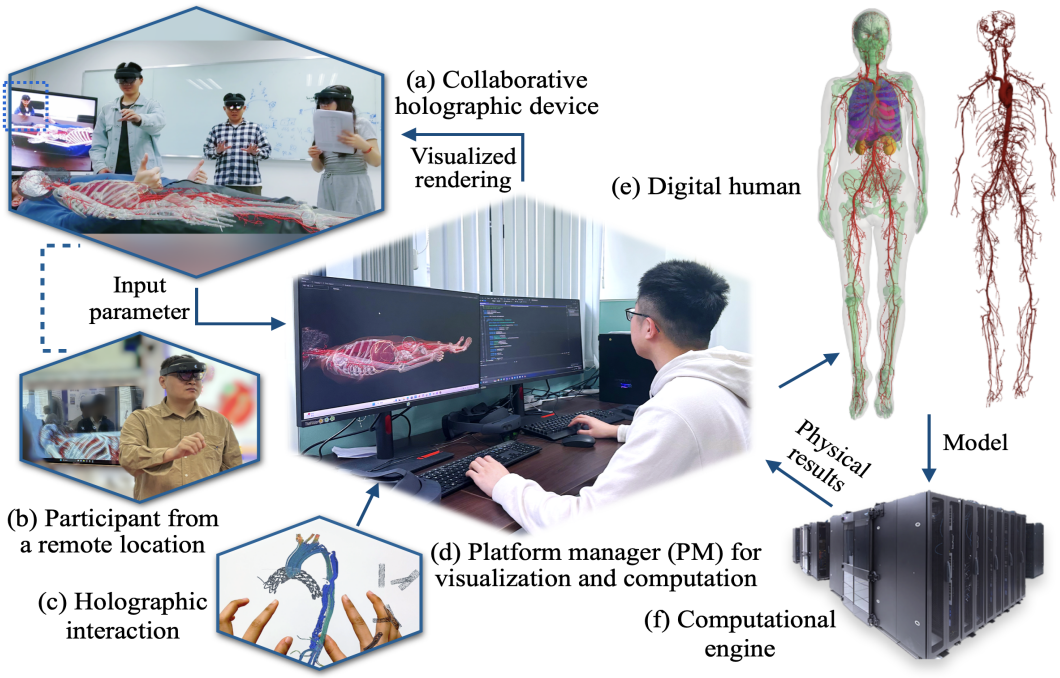

Fig. 1. The basic components of the proposed platform. (a) The configuration includes several linked MR devices with cameras. The view of the laboratory is captured by the fourth user as indicated by the blue dashed line on the screen; (b) a participant located remotely engages in the collaboration; (c) interaction with the virtual object viewed through a user's device; (d) the platform manager receives input from the holographic devices and utilizes that information to guide and manage the virtual operations; (e) a digital human body with the arterial network and various organs; (f) a parallel computer used to carry out large-scale computation in the simulation.

To support fast computations on fine meshes, in this paper, we explore a parallel domain decomposition method with high scalability when utilizing a large number of processor cores.

The segmentations of high-resolution medical images requires extensive manual efforts. Recent advancements in machine learning techniques, particularly those based on convolutional neural networks (CNNs) [24], [25], have provided a powerful solution to address this challenge. One key benefit is their ability to capture local contextual information. In CNNs, the convolutional layers utilize filters to scan the input image, enabling the network to examine local image patches and capture intricate details. This process facilitates the accurate identification of structures and boundaries present in medical images. By training deep CNN models, we are able to reconstruct the 3D geometry of the human body with sufficient accuracy and efficiency, thereby facilitating the numerical simulation proposed in this paper. This process is illustrated in Figure 3.

A. Interaction with holographic devices

MR holographic devices enable surgeons to immerse themselves in a 3D representation of patient-specific anatomy and interact with it in a dynamic and engaging way. For instance, by simply raising a hand, a function menu is activated, allowing surgeons to select the specific tools and functions required for the surgery. Furthermore, a slider screen enables easy adjustment of the level of transparency of the object, such as the virtual human skin and the aorta surface, facilitating op-

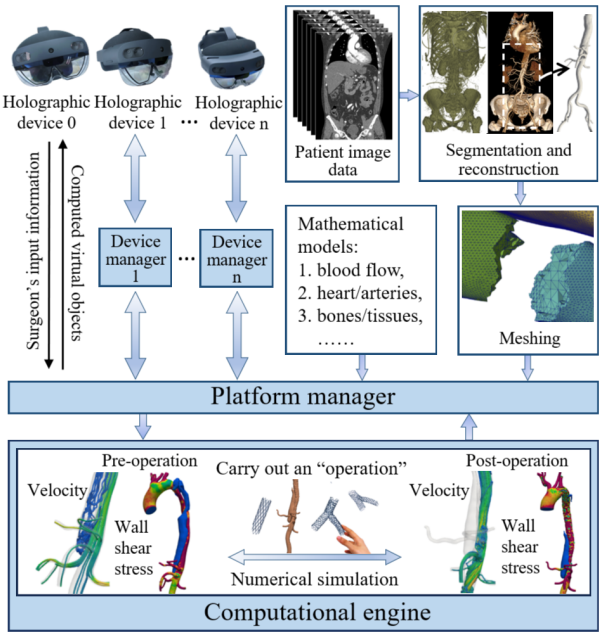

Fig. 2. Patient-specific images undergo a segmentation and reconstruction procedure to create a 3D geometry of the specific area of interest. Based on this geometry, a suitable mesh is generated and loaded along with the mathematical model to the PM. The leading device (server) transmits both physical information and operational commands to the PM, while the clients connect with the PM via their own manager to facilitate collaboration. The computational engine conducts numerical simulation and produces visualized outcomes, which are then conveyed back to the users for review.

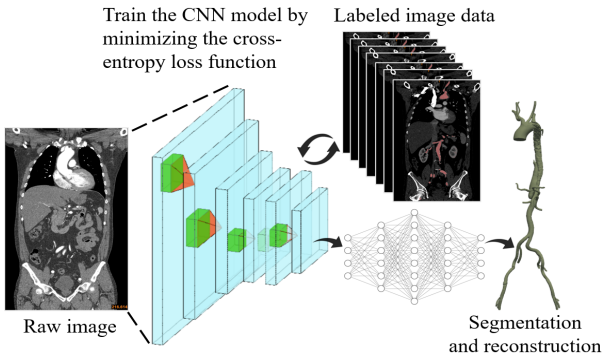

Fig. 3. Segmentation of a raw medical image using convolutional neural networks trained by labeled image data. The geometry of the artery can be reconstructed based on the segmentation results.

timal visualization of the internal structures. This allows users to fine-tune the object visibility based on their preferences and requirements.

To focus on a patient with an aortic dissection, we preload the diseased portion of the artery and the surrounding structures to the MR holographic devices from which the surgeons can precisely identify the location and extent of the dissection. Using hand-gestures, the deployment process of stents can also be visually guided to adjust their size and alignment accordingly. Once the size, the length and the angles are determined, a numerical simulation can be launched to obtain the computed flow fields. By incorporating near real-time simulation, surgeons can explore different plans and assess potential outcomes before performing the actual procedure. This virtual evaluation process significantly minimizes the risk of unintentional harm to critical structures, providing greater safety and confidence during the surgical intervention.

Additionally, MR holographic devices facilitate seamless collaboration and consultation among surgeons, whether they are physically co-located or remotely situated. By sharing the holographic representation of the surgical plan, experts can provide real-time guidance and insights, thereby enhancing the overall quality and effectiveness of the surgical procedure. This capability allows for interdisciplinary collaboration and harnesses the expertise of multiple professionals, leading to improved decision-making and better patient cares.

B. Multi-user collaborations and synchronization of devices

Each pair of holographic device has its individual coordinate system, viewing field and angle, and is controlled by the user wearing them, but in some situations, we would like others to share the same viewing field or the same object from the same angle or distance, or simply synchronize two or more devices. The synchronization process enables collaborative manipulation of a virtual object by multiple users wearing their own holographic devices. In this paper, we only consider simple operations such as rotation, scaling, and some shape modification. These interactions are achieved via a TCP connection, ensuring smooth communication between the users. Once the synchronization is established, operations performed by the leading user are simultaneously shared with all participants. Meanwhile, other users have the freedom to move the object around and observe it from different angles and locations, enhancing their overall viewing experience.

We next define some notations for collaborative manipulation. In the system, each holographic device possesses its individual virtual environment, or more precisely defined as a linear vector space $\{\mathcal{V}\}$, which is apart from the physical environment that is also a vector space denoted as $\{\mathcal{R}\}$ (which is actually the three-dimensional space we live in). Each device operates with its own coordinate system and the corresponding objects. The purpose of the synchronization process is to establish connections between the virtual environments of these holographic devices. For simplicity, we consider two devices viewing the same object represented as $\Omega_j(t) = \{\boldsymbol{x}(t) | \ \boldsymbol{x}(t) \in \mathcal{V}_j\}$, $j = 1, 2$, where $\mathcal{V}_j$ are virtual spaces generated by these two devices, respectively. Here t is a temporal parameter indicating that the shape of the object may change in time. We define a bijective mapping $\mathcal{F} : \Omega_1(t) \to \Omega_2(t)$ between the two devices. Let t be the current time, for any change of $\boldsymbol{x}(t) \in \Omega_1(t)$, the corresponding $\boldsymbol{y}(t) = \mathcal{F}(\boldsymbol{x}(t)) \in \Omega_2(t)$ is given by a combination of the following transformations:

- Translation: $\mathcal{F}(\boldsymbol{x}(t)) = \boldsymbol{y}(t-\tau) + (\boldsymbol{x}_{ct}(t) - \boldsymbol{x}_{ct}(t-\tau))$, where $\boldsymbol{x}_{ct}(t)$ is the center coordinate of the object, $t-\tau$ is the time before the transformation.
- Rotation around the center:
$$\mathcal{F}(\boldsymbol{x}(t)) = \mathcal{Q}(\boldsymbol{x}(t), \boldsymbol{x}(t-\tau)) \cdot (\boldsymbol{y}(t-\tau) - \boldsymbol{y}_{ct}(t-\tau)) + \boldsymbol{y}_{ct}(t),$$
where $\mathcal{Q}(\boldsymbol{x}(t), \boldsymbol{x}(t-\tau))$ is a rotation matrix satisfying $\boldsymbol{x}(t) - \boldsymbol{x}_{ct}(t) = \mathcal{Q}(\boldsymbol{x}(t-\tau) - \boldsymbol{x}_{ct}(t-\tau))$, which takes the form $\mathcal{Q} = \mathcal{Q}_x \mathcal{Q}_y \mathcal{Q}_z$, where
$$\mathcal{Q}_x = \begin{pmatrix} \cos\theta_x & \sin\theta_x & 0 \\ -\sin\theta_x & \cos\theta_x & 0 \\ 0 & 0 & 1 \end{pmatrix}, \ \mathcal{Q}_y = \begin{pmatrix} \cos\theta_y & 0 & \sin\theta_y \\ 0 & 1 & 0 \\ -\sin\theta_y & 0 & \cos\theta_y \end{pmatrix},$$
$$\mathcal{Q}_z = \begin{pmatrix} 1 & 0 & 0 \\ 0 & \cos\theta_z & \sin\theta_z \\ 0 & -\sin\theta_z & \cos\theta_z \end{pmatrix},$$
and $\theta_x, \theta_y, \theta_z$ are the rotation angles around the three axes, respectively.
- Scaling:
$$\mathcal{F}(\boldsymbol{x}(t)) = \alpha(\boldsymbol{x}(t), \boldsymbol{x}(t-\tau)) \cdot (\boldsymbol{y}(t-\tau) - \boldsymbol{y}_{ct}(t-\tau)) + \boldsymbol{y}_{ct}(t),$$
where the scaling factor $\alpha(\boldsymbol{x}(t), \boldsymbol{x}(t-\tau)) = (\boldsymbol{x}(t) - \boldsymbol{x}_{ct}(t))/(\boldsymbol{x}(t-\tau) - \boldsymbol{x}_{ct}(t-\tau))$.

We consider one of the users as the lead user and his/her device as the server device, and all other devices as client devices. In the current design of the system, we allow the server device to share its view of the virtual object with all clients by issuing a command called "focus". The position and the orientation of the object viewed by the client are adjusted based on the message obtained from the server, as shown in Figure 4.

We define the position of the object in the virtual environment by using a spherical coordinate system centered around the camera. The distance between the object and the camera

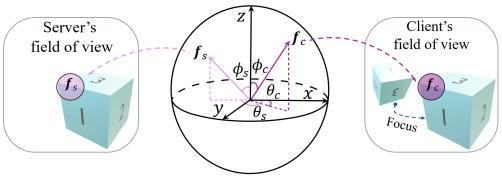

Fig. 4. The server device shares its view of the virtual object with a client by issuing a command called "focus". A mapping is defined for this operation based on the difference of the forward direction of the server camera $\boldsymbol{f}_s(t) = (r_s(t), \phi_s(t), \theta_s(t))$ and that of a client camera $\boldsymbol{f}_c(t) = (r_c(t), \phi_c(t), \theta_c(t))$.

determines the radius. The forward direction of the server camera is represented by a vector $\boldsymbol{f}_s(t) = (r_s(t), \phi_s(t), \theta_s(t))$ and that of a client camera is $\boldsymbol{f}_c(t) = (r_c(t), \phi_c(t), \theta_c(t))$. In cases where the client's perspective differs from the server's ($\boldsymbol{f}_c(t) \neq \boldsymbol{f}_s(t)$), we adjust the position of the object within the client's coordinate system to align the view with the server. Let $\boldsymbol{f}_{so}(\boldsymbol{x}(t)) = (r_{so}(\boldsymbol{x}(t)), \phi_{so}(\boldsymbol{x}(t)), \theta_{so}(\boldsymbol{x}(t)))$ be the vector pointing from the camera to the center of the object in the server's view. The difference in the viewing angles of the object between the server and the client can be calculated by $\theta_c(t) - \theta_s(t)$ and $\phi_c(t) - \phi_s(t)$, and the new position of the object in the client's spherical coordinate system involves the angles $\theta_r(\boldsymbol{x}(t)) = \theta_{so}(\boldsymbol{x}(t)) + \theta_c(t) - \theta_s(t)$ and $\phi_r(\boldsymbol{x}(t)) = \phi_{so}(\boldsymbol{x}(t)) + \phi_c(t) - \phi_s(t)$. Assuming the location of the client camera is $(x_{cam}, y_{cam}, z_{cam})$, we introduce a mapping $\mathcal{F} : \Omega_1(t) \to \Omega_2(t)$ to obtain the new position of the object in the client's view $\boldsymbol{y}(t) = (y_1(t), y_2(t), y_3(t))$ after receiving the "focus" command:

$$
\begin{aligned}
y_1(t) &= r_{so}(\boldsymbol{x}(t)) \sin(\phi_r(\boldsymbol{x}(t))) \cos(\theta_r(\boldsymbol{x}(t))) + x_{cam}(t),\\
y_2(t) &= r_{so}(\boldsymbol{x}(t)) \cos(\phi_r(\boldsymbol{x}(t))) + y_{cam}(t),\\
y_3(t) &= r_{so}(\boldsymbol{x}(t)) \sin(\phi_r(\boldsymbol{x}(t))) \sin(\theta_r(\boldsymbol{x}(t))) + z_{cam}(t).
\end{aligned}
$$

A simple case is when the server camera is directed towards the center of the object ($\boldsymbol{f}_{so}(\boldsymbol{x}(t)) = \boldsymbol{f}_s(t)$). As a result, the position of the object in the spherical coordinate system becomes simplified $\theta_r(\boldsymbol{x}(t)) = \theta_c(t)$ and $\phi_r(\boldsymbol{x}(t)) = \phi_c(t)$, which means aligning the object to the direction that client camera is facing.

C. Mathematical model of vascular flows

In this study, we employ the incompressible Navier-Stokes equations to model the blood flow in the vascular system. The computational domain of the artery is $\Omega \in \mathbb{R}^3$. Without loss of generality, Ω refers to the virtual object viewed by a single device, that is, $\Omega = \Omega_1$. The blood flow is governed by the following equations:

$$
\begin{cases}
\rho\left(\dfrac{\partial \boldsymbol{u}}{\partial t} + \boldsymbol{u}\cdot\nabla\boldsymbol{u}\right) - \nu\Delta\boldsymbol{u} + \nabla p = \boldsymbol{g}, & \text{in } \Omega\times(0,T),\\
\nabla\cdot\boldsymbol{u} = \boldsymbol{0}, & \text{in } \Omega\times(0,T),\\
\boldsymbol{u}|_{t=0} = \boldsymbol{u}_0, & \text{in } \Omega,
\end{cases}
$$

where $\boldsymbol{u}$ is the velocity, p is the pressure, ρ is the blood density, ν is the viscosity, $\boldsymbol{g}$ is the given source term, and $\boldsymbol{u}_0$ is the initial velocity. The boundary of the domain is denoted by $\partial\Omega = \Gamma_I \cup \Gamma_W \cup \Gamma_O^i$, where Γ_I, Γ_W and Γ_O^i are the inlet, the arterial wall, and the i^{th} outlet ($i = 1, 2, \cdots, m$), respectively. We impose a no-slip no-penetration boundary condition on the wall Γ_W and a three-element Windkessel model applied as the outlet boundary condition,

For the simulation, the computational domain is covered by an unstructured mesh composed of tetrahedral elements, as shown in the zoom-in figure in Figure 5. To enable parallel computation, the global mesh is further partitioned into several subdomains highlighted with different colors in the figure.

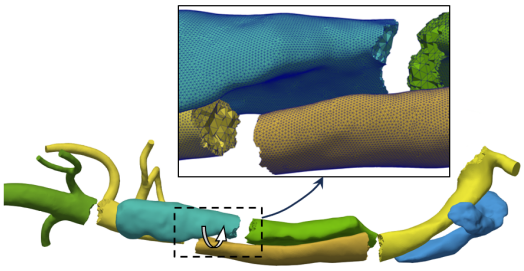

Fig. 5. Partition of the artery mesh into 7 subdomains with each color representing a subdomain. The upper subfigure displays a part of the mesh within the dashed box after slight rotation.

D. Parallel algorithms for the simulation

The blood flow model is discretized using a $P_1 - P_1$ finite element method with stabilization in space and an implicit backward Euler method in time. This discretization leads to a large-scale, sparse, and nonlinear algebraic system to be solved at each time step:

$$F(x) = 0, \tag{II.1}$$

where F is the discretized nonlinear operator and x represents the interested physical fields, such as velocity and pressure. We develop a scalable and robust algorithm based on the Newton-Krylov-Schwarz (NKS) method [23] for the algebraic system (II.1). Speficifically, an inexact Newton method is employed to solve the nonliear system, wherein a Krylov subspace method is utilized to solve the analytically computed Jacobian systems. In order to enhance the efficiency of the solution process, the restricted additive Schwarz (RAS) method is used as a preconditioner. The flowchart of the NKS algorithm is shown in Figure 6.

In the NKS algorithm, starting from an initial guess x^0 and $k = 0$, a new approximate solution x^{k+1} is updated from the current solution x^k by $x^{k+1} = x^k + \lambda^k s^k$, where λ^k is the step length calculated using a backtracking line search technique, s^k is the Newton correction step obtained by approximately solving the linear Jacobian system:

$$JM^{-1}Ms^k = -F(x^k), \tag{II.2}$$

where $J = F'(x^k)$ is the Jacobian matrix, M^{-1} is a preconditioner. The linear iteration is stopped if

$$\| JM^{-1}Ms^k + F(x^k) \| \leq \eta_k \| F(x^k) \|, \tag{II.3}$$

where η_k is a given relative tolerance. The parallel scalability of the algorithm depends on the RAS preconditioner, which is given by

$$M^{-1} = \sum_{l=1}^{np} (R_l^0)^T J_l^{-1} R_l^\delta, \tag{II.4}$$

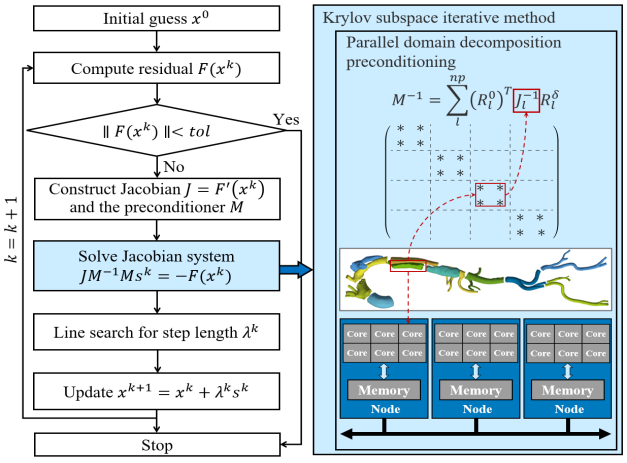

Fig. 6. The flowchart of the Newton-Krylov-Schwarz algorithm for solving the nonlinear system (II.1) at each time step. In the preconditioner, the entire problem is decomposed into many subproblems that are assigned to different processor cores and solved in parallel.

where np denotes the number of processor cores, R_l^0 is the restriction operator that maps a global vector x into the l^{th} non-overlapping subdomain, and R_l^δ is another restriction operator that corresponds to an extended subdomain with δ overlaps. J_l^{-1} represents the solve of a subdomain problem by the inverse of a submatrix. This preconditioner partitions the entire problem into many subproblems that are distributed to different processor cores and solved in parallel, leading to improved performance and reduced computational time.

III. Experiments and Discussions

In this section, we demonstrate the surgical planning process for a patient with a type B aortic dissection using the holographic device, then evaluate the outcomes of virtual surgery by conducting two numerical simulations, representing the conditions before and after the surgical procedure. When a type B aortic dissection poses a risk of rupture or leads to severe complications, prompt intervention becomes crucial. One potential treatment option involves the deployment of a stent. During this procedure, a small tube made of wire is inserted through a peripheral blood vessel, effectively sealing off the dissection and restoring the integrity of the aorta.

A. Some basic steps of surgical planning through the holographic device

We first show some basic steps in the proposed platform for the placing of a stent in a patient with aortic dissection. The steps are illustrated in Figure 7. Note that all the images in Figure 7 are captured using the camera of the device. However, due to the camera's positioning being slightly higher than the user's eye level, the physical environment may not precisely match the user's perspective in these images. For instance, the touch cursor, indicated by a small pink ring in the images, represents the position of the index finger's tip. Usually, its displayed position does not perfectly align with the actual tip of the finger.

Users have the ability to change the shape and other properties of the digital aorta with some hand gestures. Through the integration of a camera, the holographic device detects the user's hands and their interaction with the virtual environment. The user can pinch their thumb and index finger together to grab a hologram located nearby. Maintaining this gesture enables the user to hold the object, while releasing the fingers allows for releasing it. In addition to this grabbing gesture, various other manipulations are feasible, such as moving, rotating, and resizing the objects.

Pressure and velocity are crucial quantities in hemodynamics that play a pivotal role in guiding surgical planning. As shown in the first step of Figure 7, the pressure distribution can be visualized on the surface of the aorta for assessment. Furthermore, by utilizing a fluoroscopic window, one can observe the streamlines of flow inside the artery. To enhance the visualization of the aortic dissection, we have incorporated a slider that enables control over the transparency of the surface of the aorta.

The system offers a simplified and intuitive method for users to conduct virtual surgical planning. By raising the left hand, users can access an operation menu containing a range of buttons. These buttons can be customized with various functionalities to accommodate different requirements. For instance, the first button allows users to visualize the pressure distribution on the surface of the aorta. The second button presents the wall shear stress distribution. Additionally, the third button initiates the surgical planning process. These functionalities collectively provide users with a clearer understanding of the patient's condition, facilitating informed decision-making throughout the surgical planning process.

A typical treatment for type B aortic dissection is the deployment of a stent to repair the affected artery. In the virtual environment, we provide several stents specifically designed for this purpose. By selecting the third button labeled "surgical planning" in the menu, users gain access to various stents with different shapes, as illustrated in Step 4 of Figure 7. The platform offers flexible customization options, allowing users to resize all stents using intuitive gestures like stretching and compressing. By pinching a stent with two fingers, users can freely manipulate and rotate it, placing it in any desired location. The deployment process is depicted in Step 5 and Step 6 of the figure.

To evaluate the hemodynamic conditions after inserting the stent, users can choose the fourth button in the menu to perform numerical simulations utilizing patient-specific parameters and the aortic geometry. Leveraging a powerful parallel computer as the computational engine, precise numerical results can be obtained in near real-time, which are then conveyed back to the users for review. The surgical outcomes can be visualized from any perspective using the holographic device, allowing for a comprehensive comparison with the presurgery data, as illustrated in Step 8 of Figure 7.

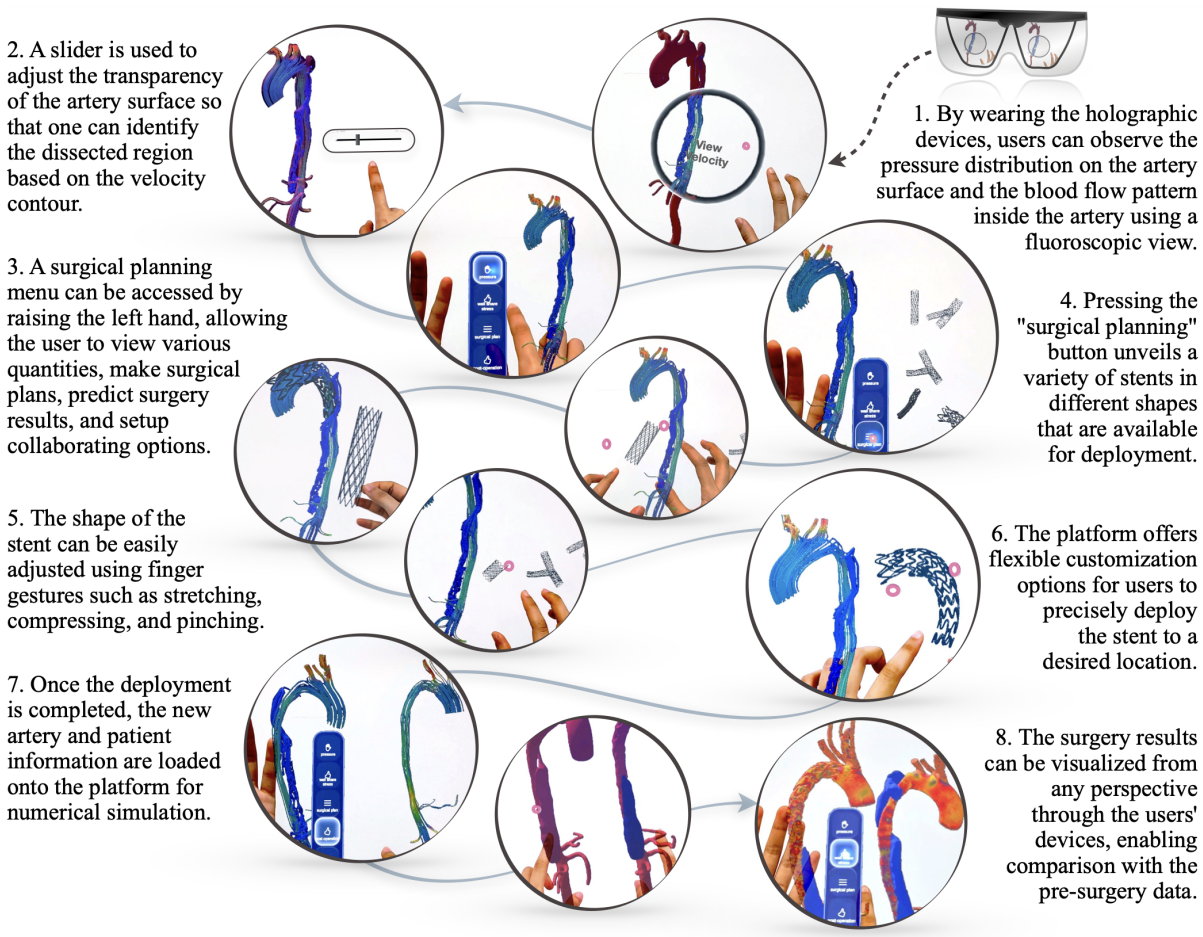

Fig. 7. An overview of the virtual surgical planning workflow using holographic devices, with a focus on the deployment of stents in the aorta.

B. Analysis of the numerical results

In this subsection, we provide more details about the simulation. For the computation of the pre- and post-operative aortic dissection, we use meshes with 4,137,704 and 3,484,367 elements, respectively, and the meshes are partitioned into 480 subdomains. The simulations are carried out using 480 processor cores. Parameters for the blood flow model are as follows: the total resistance is $R_T = 998.94\ dyns/cm^5$, the total compliance is $C_T = 5.11 \times 10^{-2}\ cm^5/dyn$, the density of the blood is $\rho = 1.06\ g/cm^3$, and the dynamic viscosity is $\nu = 0.035\ g/cms$.

To compare the hemodynamic conditions before and after the placement of the stent, we show the velocity distribution and flow pattern in the dissected aorta at peak systole in Figure 8. In both cases, the blood flow coming from the left ventricle of the heart enters the true lumen of the aorta and undergoes acceleration as it traverses the aortic arch. In the pre-operative case, blood flows into the false lumen through the rapture, posing significant risks such as thrombus formation, aneurysm expansion, and blood pressure instability. However, in the post-operative case, the deployment of a stent effectively prevents blood flow into the false lumen. As a result, the false lumen exhibits zero velocity, and its volume significantly decreases due to the removal of thrombosis. Figure 8 provides zoomed-in subfigures that illustrate the velocity streamlines in three specific areas. These subfigures demonstrate that the virtual surgery results in a smoother blood flow, with reduced or eliminated vortices in the false lumen. This indicates improved hemodynamic conditions in the aorta, providing favorable outcomes for the patient after surgery.

IV. Summary

We developed a collaborative MR platform for vascular surgery planning, the system allows multiple users to simultaneously visualize and manipulate digital objects in the human vascular system. Special hand gestures are designed and integrated into the holographic devices to facilitate the real time interaction of the users with the virtual objects whose initial geometry is obtained via the segmentation and reconstruction of the patient-specific images. After each change of the vascular geometry, a hemodynamic analysis is carried out on a parallel computer connected to the platform and the results are displayed on the glasses and discussed by the

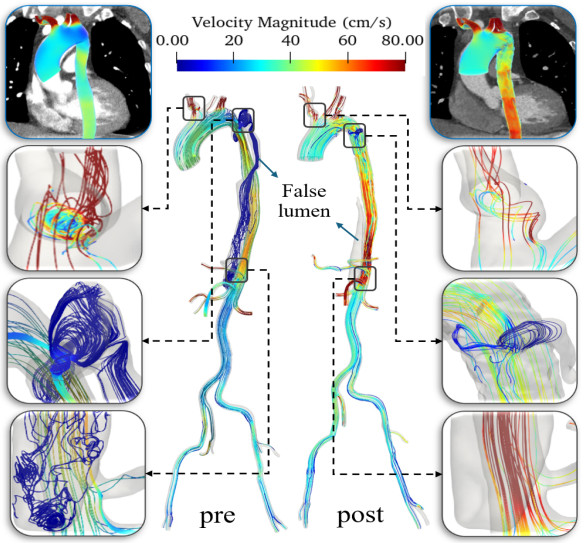

Fig. 8. A comparison of velocity contour and flow patterns in a dissected aorta at peak systole before (left column) and after (right column) of the planed surgery. Numerical results predict that the aorta has better hemodynamic conditions after the virtual surgery.

users. To showcase the applicability of the proposed platform, we present a case study for the planning of a surgery for a patient with a type B aortic dissection. The platform provides visual support for some possible deployment of stents and near real-time hemodynamic analyses. This allows surgeons to receive prompt operational feedback and assess the outcomes of different surgical plans prior to the actual surgery.

REFERENCES

[1] M. Hanna, I. Ahmed, J. Nine, S. Prajapati, and L. Pantanowitz, "Augmented reality technology using Microsoft hololens in anatomic pathology," *Archives of pathology laboratory medicine*, vol. 142, pp. 638–344, 2018.

[2] R. Serrano Vergel, P. Morillo Tena, S. Casas Yrurzum, and C. Cruz-Neira, "A comparative evaluation of a Virtual Reality table and a HoloLens-based augmented reality system for anatomy training," *IEEE Transactions on Human-Machine Systems*, vol. 50, no. 4, pp. 337–348, 2020.

[3] M. Venkatesan, H. Mohan, J. Ryan, C. Schürch, G. Nolan, D. Frakes, and A. Coskun, "Virtual and augmented reality for biomedical applications," *Cell Reports Medicine*, vol. 2, no. 7, p. 100348, 2021.

[4] K. Matwala, T. Shakir, C. Bhan, and M. Chand, "The surgical metaverse," *Cirugía Española (English Edition)*, 2023.

[5] Y. Daineko, M. Ipalakova, D. Tsoy, B. Alipova, A. Kozhakhmetov, and A. Mustafina, "Towards metahospital: augmented and virtual reality in medicine," *Procedia Computer Science*, vol. 231, pp. 373–378, 2024.

[6] M. Ammendola, F. Vescio, M. A. Ansari, J. Hila, L. Rizzo, R. Romano, F. Marchegiani, N. de'Angelis, T. Piardi, D. Cavaliere, A. E. Frampton, T. M. H. Gall, M. Luposella, R. Memeo, G. Navarra, S. Curcio, and G. Currò, "Metaverse and telementoring: From surgery to workshop," *Surgical Innovation*, vol. 31, no. 2, pp. 212–219, 2024.

[7] J. Wang, Y. Zhao, X. Xu, Q. Wang, F. Li, S. Zhang, Z. Gan, R. Xiong, J. Zhang, and X. Chen, "A patient-specific, interactive, multiuser, online mixed-reality neurosurgical training and planning system," *Neurosurgical Focus*, vol. 56, no. 1, p. E15, 2024.

[8] M. Petersen, J. Mlakar, S. Haber, M. Parent, Y. Smith, P. Strick, M. Griswold, and C. McIntyre, "Holographic reconstruction of axonal pathways in the human brain," *Neuron*, vol. 104, no. 6, pp. 1056–1064.e3, 2019.

[9] Y. Gong, F. Qi, J.-Y. Wang, Y. Liu, T. Ma, Z. Cheng, Y. Jiang, R. Chen, X. Wang, L. Luo, and X.-C. Cai, "An interactive platform for a high performance digital twin of a human heart," in *2023 IEEE International Conference on Metaverse Computing, Networking and Applications*, 2023, pp. 193–200.

[10] E. Checcucci, D. Amparore, G. Volpi, S. De Cillis, F. Piramide, P. Verri, A. Piana, M. Sica, C. Gatti, P. Alessio, A. Quarà, M. Burgio, M. Colombo, G. Busacca, A. Mottrie, E. Cherullo, A. Breda, A. Antonelli, R. Bollens, A. Minervini, J. Porter, R. Schiavina, R. Autorino, A. Tewari, M. Di Dio, C. Fiori, and F. Porpiglia, "Metaverse surgical planning with three-dimensional virtual models for minimally invasive partial nephrectomy," *Eur Urol*, vol. 85, no. 4, pp. 320–325, 2023.

[11] A. Acar, J. Atoum, A. Reed, Y. Li, N. Kavoussi, and J. Y. Wu, "Intraoperative gaze guidance with mixed reality," *Healthcare Technology Letters*, vol. 00, pp. 1–8, 2023.

[12] H. Bai, P. Sasikumar, J. Yang, and M. Billinghurst, "A user study on mixed reality remote collaboration with eye gaze and hand gesture sharing," 2020, pp. 1–13.

[13] V. Chheang, D. Schott, P. Saalfeld, L. Vradelis, T. Huber, F. Huettl, H. Lang, B. Preim, and C. Hansen, "Advanced liver surgery training in collaborative vr environments," *Computers & Graphics*, vol. 119, p. 103879, 2024.

[14] V. Chheang, P. Saalfeld, F. Joeres, C. Boedecker, T. Huber, F. Huettl, H. Lang, B. Preim, and C. Hansen, "A collaborative virtual reality environment for liver surgery planning," *Computers & Graphics*, vol. 99, pp. 234–246, 2021.

[15] V. Chheang, P. Saalfeld, T. Huber, F. Huettl, W. Kneist, B. Preim, and C. Hansen, "Collaborative virtual reality for laparoscopic liver surgery training," 2019, pp. 1–17.

[16] K. Malukhin and K. Ehmann, "Mathematical Modeling and Virtual Reality Simulation of Surgical Tool Interactions With Soft Tissue: A Review and Prospective," *Journal of Engineering and Science in Medical Diagnostics and Therapy*, vol. 1, no. 2, p. 020802, 2018.

[17] M. Jing, Z. Cui, H. Fu, and X. Chen, "Real-time deformation simulation of kidney surgery based on virtual reality," *Journal of Shanghai Jiaotong University (Science)*, vol. 26, no. 3, pp. 290–297, 2021.

[18] S. Qin, R. Chen, B. Wu, and X.-C. Cai, "A highly parallel fully implicit domain decomposition method for the simulation of the hemodynamics of a patient-specific artery at the full-body scale," *Journal of Computational Physics*, vol. 472, p. 111730, 2023.

[19] Z. Lin, R. Chen, B. Gao, S. Qin, B. Wu, J. Liu, and X.-C. Cai, "A highly parallel simulation of patient-specific hepatic flows," *International journal for numerical methods in biomedical engineering*, vol. 37, no. 6, p. e3451, 2021.

[20] S. Qin, R. Chen, B. Wu, W.-S. Shiu, and X.-C. Cai, "Numerical simulation of blood flows in patient-specific abdominal aorta with primary organs," *Biomechanics and Modeling in Mechanobiology*, vol. 20, no. 3, pp. 909–924, 2021.

[21] C. Ong, I. Wee, N. Syn, S. Ng, H. Leo, A. Richards, and A. Choong, "Computational fluid dynamics modeling of hemodynamic parameters in the human diseased aorta: A systematic review," *Annals of Vascular Surgery*, vol. 63, pp. 336–381, 2019.

[22] F. Kong, V. Kheyfets, E. Finol, and X.-C. Cai, "An efficient parallel simulation of unsteady blood flows in patient-specific pulmonary artery," *International Journal for Numerical Methods in Biomedical Engineering*, vol. 34, no. 4, p. e2952, 2018.

[23] L. Luo, W.-S. Shiu, R. Chen, and X.-C. Cai, "A nonlinear elimination preconditioned inexact newton method for blood flow problems in human artery with stenosis," *Journal of Computational Physics*, vol. 399, p. 108926, 2019.

[24] L. Gu and X.-C. Cai, "Fusing 2D and 3D convolutional neural networks for the segmentation of aorta and coronary arteries from CT images," *Artificial Intelligence in Medicine*, vol. 121, p. 102189, 2021.

[25] L. Gu, W. Zhang, J. Liu, and X.-C. Cai, "Decomposition and composition of deep convolutional neural networks and training acceleration via sub-network transfer learning," *Electronic Transactions on Numerical Analysis*, vol. 56, pp. 157–186, 2022.